Title
Dopant-Free Partial Rear Contacts Enabling 23% Silicon Solar Cells

Journal
Advanced Energy Materials, 9(9)

ISSN
1614-6832

Authors
Bullock, James
Wan, Yimao
Hettick, Mark
et al.

Publication Date
2019-03-01

DOI
10.1002/aenm.201803367

Peer reviewed

DOI: 10.1002/

Article type: Full paper

Title: Dopant-Free Partial Rear Contacts Enabling 23% Silicon Solar Cells

James Bullock, Yimao Wan, Mark Hettick, Xu Zhaoran, Sieu Pheng Phang, Di Yan, Hanchen Wang, Wenbo Ji, Chris Samundsett, Ziv Hameri, Daniel Macdonald, Andres Cuevas and Ali Javey[*]

Dr. J. Bullock, Dr. Y. Wan, M. Hettick, X. Zhaoran, H. Wang, W. Ji, Prof. A. Javey

Department of Electrical Engineering and Computer Sciences, University of California, Berkeley, California 94720, USA
Materials Sciences Division, Lawrence Berkeley National Laboratory, Berkeley, California 94720, USA.
Email: ajavey@berkeley.edu

Dr. Y. Wan, Dr. S. P. Phang, Dr. D. Yan, C. Samundsett, Prof. D. Macdonald, Prof. A. Cuevas

Research School of Engineering, The Australian National University (ANU), Canberra, Australian Capital Territory 2602, Australia.
Dr. Z. Hameri

University of New South Wales, Kensington, New South Wales 2052, Australia.

Keywords: Titanium oxide, selective contacts, silicon photovoltaics

Abstract

Over the past five years there has been a significant increase in both the intensity of research and the performance of crystalline silicon devices which utilize metal compounds to form carrier-selective heterocontacts. Such heterocontacts are less fundamentally limited and have the potential for lower costs compared to the current industry dominating heavily-doped, directly-metalized contacts. Here we present a low temperature (≤ 230°C), TiO_x / LiF_x / Al electron heterocontact, which achieves mΩcm^2 scale contact resistivities ρ_c on lowly doped n-type substrates. As an extreme demonstration of the potential of this heterocontact, we trial it in a newly developed, high efficiency n-type solar cell architecture as a partial rear contact (PRC). Despite only contacting ~1% of the rear surface area, an efficiency of greater than 23% is achieved, setting a new benchmark for n-type solar cells featuring undoped PRCs and confirming the unusually low ρ_c of the TiO_x / LiF_x / Al contact. Finally, in contrast to previous versions of the n-type undoped PRC cell, the performance of this cell is maintained after annealing at 350-400°C, suggesting its compatibility with conventional surface passivation activation and sintering steps.

1. Introduction

Recent advancements in carrier-selective heterocontacts for crystalline silicon (c-Si) photovoltaics (PV) have highlighted opportunities for utilization of materials-based approaches in improving the performance of this technology. For example, materials such as metal oxides, nitrides and fluorides have been demonstrated to form electron and hole selective interfaces when applied to c-Si.[1–7] Such an approach has potential benefits over conventional heavily-doped direct-metallization approaches; including lower processing temperatures, simpler contact formation and the removal of fundamental limitations, such as Auger recombination and free carrier absorption.[8,9] In addition, the unique interface properties of some metal compound / c-Si interfaces have even enabled novel solar cell architectures, for example, n-type c-Si cells with undoped partial rear contacts (PRC).[10,11] This specific architecture utilizes a near-ideal surface passivation layer, such as hydrogenated silicon nitride SiN_x,[12] to cover the vast majority of the rear surface which can greatly reduce the average surface recombination factor J_0 and increase the rear reflection. Only a small percentage of the area is contacted, typically <5%, where electrons flow to be collected. An n-type undoped PRC cell structure was not previously attainable due to the tendency of n-type c-Si to form an interface potential barrier under direct metallization, which resulted in prohibitively high contact resistivity ρ_c. The first successful demonstration of this cell came after a breakthrough in low resistance interfaces to n-type c-Si with a low work function LiF_x / Al

electrode. This contact was used to fabricate an undoped PRC cell attaining an efficiency of 20.6% with a PRC covering only ~1% of the rear surface.[11] The next evolutionary step in this cell structure was the integration of a passivation layer at the PRC interface. This came with the introduction of a TiO_x / Ca / Al contact,[10] which was found to provide both reduced surface recombination and low contact resistivity, enabling an efficiency of 21.8%. Following on from these early developments, there exist three major avenues to easily improve the electron PRC: *i*.) reduction in the PRC interface recombination and resistivity; *ii*.) increase in the PRC material's stability to thermal and humidity stressors; and *iii*.). increasing the rear surface reflectivity via appropriate choice of PRC materials.

This paper introduces the next in this family of carrier selective interfaces, which targets the abovementioned three issues. To address this a TiO_x / LiF_x / Al heterocontact is developed and integrated into a PRC cell shown in Figure 1a. The individual materials in this contact provide several potential benefits. Firstly, TiO_x layers have been shown to provide excellent surface passivation of c-Si and have exhibited stability in some harsh environments.[13–16] It has also been experimentally demonstrated that TiO_x interlayers can increase the 'S-factor' (reduce the Fermi level pinning) as compared to directly metalized surfaces.[17] Secondly, the low work function LiF_x / Al electrode,[18] combined with the high permittivity TiO_x, can assist in the reduction of barrier heights or even lead to electron accumulation at the c-Si surface. Finally, unlike other low work function electrodes, such as Mg or Ca, LiF_x / Al

can provide near-ideal rear-reflection especially when separated from the c-Si absorber with a dielectric spacer (a quantification of this advantage is included in supplementary material S1). The unique properties of this heterocontact allows the fabrication of a c-Si cell featuring an undoped PRC which achieves a conversion efficiency of above 23% and exhibits thermal stability up to 400ºC.

2. Results and Discussion

To initially assess the performance of the TiO_x / LiF_x / Al heterocontact a series of contact recombination J_0 and resistivity ρ_c test structures are fabricated. Figure 1b shows the J_0 values attainable when passivating c-Si with different thicknesses of TiO_x (1.5, 3 and 6 nm via atomic layer deposition at 230ºC). A clear decrease in J_0 with increasing thickness is seen, as is found for many nm-scale thin films on c-Si. Figure 1c presents extractions of ρ_c for the same three TiO_x thicknesses under a thermally evaporated LiF_x (~1 nm) / Al low work-function electrode. For each TiO_x thickness the results from three separate samples are shown, with the box conveying the variation and the middle line providing the average value. Greater relative variation in ρ_c is seen for thinner TiO_x samples, likely associated with difficulties in exactly replicating nm-scale thicknesses required for the TiO_x and LiF_x layers. Reference lines for LiF_x / Al and direct Al contacts are included at the bottom and top of the plot, respectively. A clear

increase in ρ_c with the thickness of the TiO_x layer is seen, likely a result of the large bulk resistivity of TiO_x. Supplementary data provided in Figure S2a also shows that the addition of the LiF_x interlayer is found to be essential in reducing ρ_c for all thicknesses of TiO_x. The results of Figure 1b and c suggest that by controlling the thickness of TiO_x a family of heterocontacts may be accessed with ρ_c / J_0 combinations that are suitable for cells with either large-area contacts (low J_0, moderate ρ_c) or small-area contacts (low ρ_c, moderate J_0).

The second avenue to improve on the performance of previous undoped PRC generations is to increase the thermal stability. Figure 2a shows the extracted ρ_c of a set of TiO_x / LiF_x / Al heterocontacts as a function of annealing temperature. Interestingly, with increasing anneal temperature, a clear decrease in ρ_c occurs for heterocontacts with all three thicknesses of TiO_x, particularly for thicker TiO_x films. This is in contrast to a control sample with 0 nm of TiO_x, provided in the supporting information S2b, which shows an increase in ρ_c at temperatures above 150°C. This suggest that the TiO_x / LiF_x / Al contact offers a significant advantage over direct LiF_x / Al contacts in terms of thermal stability, this is particularly relevant for PRC designs where the importance of ρ_c is increased. Similarly, the TiO_x / LiF_x / Al heterocontacts are also found to be stable under humidity conditions. Figure 2b shows the measured ρ_c of TiO_x / LiF_x / Al heterocontacts taken before and after exposure to 1000 hours of 85°C and 85% relative humidity (*RH)*. The results are provided for all three TiO_x thicknesses for samples both with and without a

pre-anneal step (250°C for 10 minutes). In all cases no catastrophic changes are measured, with most points falling within the range of error of their unexposed counterparts.

To further explore the role of the TiO_x layer, a series of materials-based measurements were performed. Figure 3a shows the valence band (*i*) and secondary electron cut-off (SEC) (*ii*) spectrums of the as-deposited TiO_x layer, measured via X-ray photoelectron spectroscopy (XPS). We note that a TiO_x layer of ~12 nm was used in these measurements to avoid issues with the XPS sampling depth. A clear band tail is observed in the valence band spectrum, indicative of amorphous / nanocrystalline films (as expected from our previous studies on TiO_x)[19], but no sub-band gap defect band is seen between the valence band and Fermi energy (E_v-E_F of >3 eV). The SEC plot shows that the as-deposited TiO_x layer has a work function of ~3.8 eV, in alignment to that found in previous studies for ex-situ films.[20] These can be combined with spectroscopic ellipsometry measurements to make an estimation of the band position relative to c-Si. The refractive index of the TiO_x film, extracted with a Tauc-Lorentz model,[21] is shown in Figure 3b and reveals an optical bandgap of ~3.35 eV, similar to that measured for thin TiO_x films previously.[22] These results suggest the TiO_x layer is n-type and the expected band alignment with c-Si would present a small conduction band offset and a large valence band offset—promoting the selective collection of electrons.

To investigate the measured decrease in ρ_c with annealing, Figure 2c shows the evolution of the Ti 2p core levels for three TiO_x films: *i.*) as-deposited TiO_x; *ii.*) TiO_x / LiF_x / Al heterocontact after wet chemical removal of the LiF_x / Al layer; and *iii.*) 300°C annealed TiO_x / LiF_x / Al heterocontact after wet chemical removal of the LiF_x / Al layer. The as-deposited TiO_x film spectrum can be fit well using only the 2p doublet Ti^{4+} oxidation state suggesting that it is largely stoichiometric. This stoichiometry is also maintained after depositing, and subsequently removing, the LiF_x / Al layer. However, after annealing with a LiF_x / Al layer on top at 300°C, a slight reduction in the TiO_x film is indicated by the appearance of a small contribution from Ti^{3+} oxidation states. The reduction of TiO_x, due to interaction with an overlying layer, leading to the formation of oxygen vacancies, has been highlighted as an important factor in other TiO_x heterocontacts on c-Si.[10,23] A slight shift in the 2p doublet towards lower binding energy is also seen after depositing the LiF_x / Al overlayer and annealing. Similarly, this could be caused by a reduction in the TiO_x layer or by extrinsic doping due to interface mixing with the LiF_x layer. Both of these mechanisms may lead to a decreased bulk resistivity of the TiO_x layer, which in turn could be partially responsible for the measured decrease in ρ_c with annealing.

To test how effectively these contact properties can be transferred to operating devices, the TiO_x / LiF_x / Al heterocontacts are trialled as a small area fraction (~1%) PRC in an n-type cell. Figure 4a shows the simulated efficiency (coloured contours) of an idealized PRC cell as a function of the J_0

and ρ_c of the rear contact. The black lines on this plot represent the ideal fraction with which to apply a given J_0 and ρ_c combination. The superimposed data points, taken from the estimated values in Figures 1, suggest that the thin TiO_x layer (1.5 nm) is appropriate for a 1% PRC architecture. As highlighted above, an additional possibility not explored here is to use the thicker TiO_x layers as larger area (or even full-area) rear contacts. The thin TiO_x PRC is tested by integrating it into a 2×2 cm^2, n-type cell with an optimized front-side (the cross-sectional structure of which is depicted in Figure 1a). Figure 4b shows the current density – voltage (*JV*) plot of the champion cell, measured under standard 1-Sun conditions (100 mW/cm^2, 25°C, AM 1.5G spectrum). This cell achieves a conversion efficiency of 23.1% —the highest value for this cell class to date. The obtained open circuit voltage V_{oc} of 696 mV suggest that some level of surface recombination suppression has been maintained at the heterocontact after the anneal. This value is also confirmed by Suns-V_{oc} measurements, shown in the form of a pseudo-*JV* curve, as a dotted line in Figure 4b. The comparison between the real and pseudo *JV* curves of Figure 4b, which indicates the magnitude of series resistance R_s in the cell, suggests that efficiencies of closer to 24% could be achieved by reducing R_s. Regardless, the measured fill factor *FF* of 80% is high given the infancy of the structure and confirms that a low ρ_c has been attained at the PRC. Perhaps the most impressive parameter is the short circuit current density J_{sc}, reaching 41.5 mA/cm^2, which falls just below the maximum expected for this cell design. This high J_{sc} would not be

possible without excellent rear-reflection, a clear indication of the performance of the TiO_x / LiF_x / Al rear-reflector when combined with the SiN_x dielectric spacer. It is important to note that in comparison to previous n-type cells with undoped PRCs, the above presented cell also benefits from significant optimization of other cell regions. For example, the near-ideal front-side metallization design, shown in the inset of Figure 4d, minimizes both optical and electrical losses (more details on the cell preparation can be found in the experimental section). Figure 3c provides an accompanying quantum efficiency analysis showing the external quantum efficiency (EQE), reflection (R) and internal quantum efficiency (IQE). A comparison J_{sc} is obtained from the integrated EQE and AM 1.5G product, with a value of 41.4 mA/cm^2 in excellent agreement with the value obtained via light *JV*. After accounting for reflection, an IQE of ~100% is maintained from 300 nm to just before the band edge at 1100 nm – a clear indication of near-ideal carrier collection. The dopant diffused counterpart of this cell is an n-type Passivated Emitter Rear Locally diffused (nPERL) cell which features heavily phosphorus doped localized contacts at the rear. In comparison to this structure, the TiO_x / LiF_x / Al nPRC removes the necessity of the high temperature phosphorus diffusion as well as PRC masking and alignment steps, a significant advantage for this structure.

A crucial component in the success of these cells was post-fabrication annealing. As shown in Figure 5a, a significant improvement in *FF* is seen after annealing cells for 10 minutes in forming gas (5% H_2 : 95% N_2) within a

quartz furnace with a set temperature of 350°C – a condition chosen to mimic the thermal stress of 300°C hotplate exposure. Utilizing a forming gas anneal at the end of cell fabrication has become standard step for diffused junction c-Si solar cells (see, for example, Ref[24]) with benefits including surface passivation activation and contact sintering. Annealing beyond 10 minutes at 350°C lead to only minimal additional change. The *FF* improvement is likely resultant from simultaneous reductions in the front and rear-side contact resistance. This is in line with the known benefits of sintering electroplated silver contacts (which are used in the front-side metallization). To further investigate the thermal stability of the TiO_x / LiF_x / Al heterocontact, a representative undoped PRC cell was subjected to additional anneal testing at 350°C for 180 minutes. As shown in Figure 4b, no significant change in cell performance was seen over this period and even after an additional 10 minute anneal at a 400°C set temperature. At higher temperatures (450°C and above) the performance of the cell degrades rapidly, behaviour which is likely resultant from performance degradation in multiple cell regions (i.e. not just the rear TiO_x / LiF_x / Al PRC). Regardless, the stability exhibited in the 350-400°C range suggests the compatibility of this heterocontact structure with conventional forming gas anneal steps utilized for surface passivation and contact sintering.

3. Conclusion

In this study we have introduced the next iteration in a fast-improving family of electron heterocontacts for c-Si solar cells based on a TiO_x / LiF_x / Al layer stack. This heterocontact exhibits low contact resistivity, the possibility of surface passivation, and excellent thermal and humidity stability. To test its effectiveness, it is integrated into a newly developed n-type cell architecture, as an undoped PRC covering just ~1% of the rear surface area. This optimized 2×2 cm^2 cell has been demonstrated with an efficiency of above 23% - a new record for this architecture and for cells employing TiO_x based electron contacts in general. Further, this cell maintains its performance after annealing at temperatures up to 400°C, suggesting its compatibility with standard passivation and sintering anneal steps. These results set a new target for efficiency and thermal stability of the n-type undoped PRC cell and highlight its potential as a high efficiency cell concept.

4. Experimental Section

Contact and cell fabrication and characterization: Lifetime samples, utilized for the J_0 extraction, were fabricated on 1 Ωcm n-type, (100), float zone, c-Si wafers. After standard Radio Corporation of America (RCA) cleaning procedures, samples are dipped in a dilute (~5%) hydrofluoric acid solution, rinsed and deposited symmetrically with TiO_x layers of different thicknesses. The TiO_x layer is deposited via atomic layer deposition (ALD, Beneq TFS 200) at a temperature of 230°C, using alternating cycles of titanium tetraisopropoxide (TTIP) and water. A growth rate of ~0.3 Å/cycle is obtained for this process with 50, 100 and 200 cycles corresponding to the 1.5, 3 and 6 nm films. The effective lifetime of samples is measured after deposition using photoconductance decay (Sinton WCT 120) and the J_0 is extracted using the Kane and Swanson method.[25] It should be noted that the extracted J_0 value may change after the deposition of the LiF_x / Al layer and subsequent annealing, they are included here as an estimate.

Contact resistivity samples are fabricated in an identical manner to lifetime samples, except that TiO_x is only deposited on one surface of the 1 Ωcm n-type wafer. Following this, a LiF_x (~1 nm) / Al (~200 nm) stack is deposited via thermal evaporation through a shadow mask to define a transfer-length-method (TLM) pattern. Each TLM strip is isolated via mechanical cleaving on either side to reduce lateral spreading. Measurements of resistance versus pad spacing are made with a Keithley 2400 source-meter. It should be noted that the accuracy of the TLM approach is compromised when applied to lowly

doped wafers, as is the case here. The parallel resistance through the TiO_x layer is assumed to be negligible. Annealing was performed using sequential 10 minute anneals at temperatures between 100°C and 300°C by placing samples directly on a hotplate in air. Humidity exposure for 1000 hours at 85°C 85% *RH* was performed in an Espec LHU environmental chamber.

The 2×2 cm^2 n-type undoped PRC cells were fabricated with a double boron diffusion on the front to create localized heavily doped p^{++} regions under the front metal contacts. These front contacts, which only take up ~1% of the front surface, are defined by photolithography followed by thermal evaporation of a Cr / Pd / Ag stack and lift-off. The stack is thickened via Ag electroplating to reduce the front-side series resistance. An AlO_x / SiN_x passivation and antireflection stack is deposited on the front via ALD and plasma enhanced chemical vapor deposition (PECVD, Oxford PlasmaLab 100), respectively. A rear-side PECVD SiN_x passivation / dielectric spacer is patterned with small 30 µm diameter holes to the c-Si surface covering less than 1% of the rear surface area. Through these holes the TiO_x (1.5 nm) / LiF_x / Al stack directly contacts the n-type c-Si surface forming the PRC. Following fabrication, the whole cell structure is annealed in a quartz furnace at a set temperature of 350°C for 30 minutes in forming gas (5% H_2, 95% N_2). This anneal step was chosen to mimic the conditions of a 300°C hotplate anneal and was found to result in the highest *FF* without impacting the V_{oc}. Thermal stressing tests were performed in the same furnace at higher set temperatures.

The 1-Sun *JV* analysis was performed using a Sinton FCT450 under standard conditions (100 mW/cm^2, 25ºC, AM 1.5G spectrum), the inner edge of the contact periphery, shown Figure in 4d's inset, was used to define the cell area. Suns-V_{oc} measurements of the cells were taken on a Sinton Suns- V_{oc} tester. The EQE was measured in a PV Measurements system (model QF/IPCE) with a small sampling area that included a representative percentage of metal finger coverage. Reflection measurements were taken over a large part of the cell area using a Perkin Elmer 1050 spectrophotometer UV-visible spectrophotometer. Solar cell simulations were performed with Quokka2.0,[26] utilizing idealized values for all cell regions except the rear contact.

Materials characterization: Three XPS samples were fabricated on highly doped, single-side polished, n-type c-Si wafers. A 12 nm thick TiO_x layer is deposited on the polished side of all three samples using the same method as above. Following this, two of the three samples are coated with an additional LiF_x (~1nm) / Al stack, one of which is then annealed at 300ºC for 10 minutes on a hotplate in air. Al and LiF_x layers were etched prior to XPS measurements using a dilute hydrochloric acid solution at room temperature, following which they are rinsed thoroughly in deionized water.

XPS characterization was performed using a Kratos AXIS spectrometer with hemispherical analyzer and monochromatic Al source. Charge correction was

performed using a C 1s reference, and peak positions were fit via Voigt lineshapes and referenced to the NIST XPS database.[27] An accelerating bias of 9.0V is used for the secondary electron cut-off measurement.

Spectroscopic ellipsometry measurements were performed on a J.A. Woollam M-2000 ellipsometer. A Tauc-Lorentz model was used to extract the optical bandgap and refractive index.

Supporting Information

Supporting Information is available from the Wiley Online Library or from the author.

Acknowledgements

Materials characterization was supported by the Electronic Materials Programs, funded by the Director, Office of Science, Office of Basic Energy Sciences, Material Sciences and Engineering Division of the US Department of Energy under Contract No. DE-AC02-05CH11231. XPS characterization was performed at the Joint Center for Artificial Photosynthesis, supported through the Office of Science of the US Department of Energy under Award Number DE-SC0004993. Work at the Molecular Foundry was supported by the Office of Science, Office of Basic Energy Sciences, of the US Department of Energy (Contract No. DE-AC02-05CH11231).

Received: ((will be filled in by the editorial staff))
Revised: ((will be filled in by the editorial staff))
Published online: ((will be filled in by the editorial staff))

References

1. Bivour, M., Temmler, J., Steinkemper, H. & Hermle, M. Molybdenum and tungsten oxide: High work function wide band gap contact materials for hole selective contacts of silicon solar cells. *Sol. Energy Mater. Sol. Cells* **142**, 34–41 (2015).
2. Bullock, J., Cuevas, A., Allen, T. & Battaglia, C. Molybdenum oxide MoOx: A versatile hole contact for silicon solar cells. *Appl. Phys. Lett.* **105**, (2014).
3. Nagamatsu, K. A. *et al.* Titanium dioxide/silicon hole-blocking selective contact to enable double-heterojunction crystalline silicon-based solar cell. *Appl. Phys. Lett.* **106**, 123906 (2015).
4. Yang, X. *et al.* Tantalum Nitride Electron-Selective Contact for Crystalline Silicon Solar Cells. *Adv. Energy Mater.* **0**, 1800608
5. Wan, Y. *et al.* Magnesium Fluoride Electron-Selective Contacts for Crystalline Silicon Solar Cells. *ACS Appl. Mater. Interfaces* **8**, 14671–14677 (2016).
6. Battaglia, C. *et al.* Hole Selective MoO_x Contact for Silicon Solar Cells. *Nano Lett.* **14**, 967–971 (2014).

7. Bullock, J. *et al.* Stable Dopant-Free Asymmetric Heterocontact Silicon Solar Cells with Efficiencies above 20%. *ACS Energy Lett.* 508–513 (2018). doi:10.1021/acsenergylett.7b01279
8. Baker-Finch, S. C., McIntosh, K. R., Yan, D., Fong, K. C. & Kho, T. C. Near-infrared free carrier absorption in heavily doped silicon. *J. Appl. Phys.* **116**, (2014).
9. Richter, A., Glunz, S. W., Werner, F., Schmidt, J. & Cuevas, A. Improved quantitative description of Auger recombination in crystalline silicon. *Phys. Rev. B* **86**, 165202 (2012).
10. Allen, T. G. *et al.* A Low Resistance Calcium/Reduced Titania Passivated Contact for High Efficiency Crystalline Silicon Solar Cells. *Adv. Energy Mater.* **7**, 1602606 (2017).
11. Bullock, J. *et al.* Lithium Fluoride Based Electron Contacts for High Efficiency n-Type Crystalline Silicon Solar Cells. *Adv. Energy Mater.* **6**, 1600241 (2016).
12. Wan, Y., McIntosh, K. R., Thomson, A. F. & Cuevas, A. Low Surface Recombination Velocity by Low-Absorption Silicon Nitride on c-Si. *IEEE J. Photovolt.* **3**, 554–559 (2013).
13. Thomson, A. F. & McIntosh, K. R. Light-enhanced surface passivation of TiO2-coated silicon. *Prog. Photovolt. Res. Appl.* **20**, 343–349
14. Liao, B., Hoex, B., Aberle, A. G., Chi, D. & Bhatia, C. S. Excellent c-Si surface passivation by low-temperature atomic layer deposited titanium oxide. *Appl. Phys. Lett.* **104**, 253903 (2014).

15. Bae, D., Seger, B., Vesborg, P. C. K., Hansen, O. & Chorkendorff, I. Strategies for stable water splitting via protected photoelectrodes. *Chem. Soc. Rev.* **46**, 1933–1954 (2017).
16. Alén, P., Vehkamäki, M., Ritala, M. & Leskelä, M. Diffusion Barrier Properties of Atomic Layer Deposited Ultrathin Ta_2O_5 and TiO_2 Films. *J. Electrochem. Soc.* **153**, G304–G308 (2006).
17. Agrawal, A. *et al.* Fermi level depinning and contact resistivity reduction using a reduced titania interlayer in n-silicon metal-insulator-semiconductor ohmic contacts. *Appl. Phys. Lett.* **104**, 112101 (2014).
18. Bullock, J. *et al.* Efficient silicon solar cells with dopant-free asymmetric heterocontacts. *Nat. Energy* **1**, 15031 (2016).
19. Yin, X. *et al.* 19.2% Efficient InP Heterojunction Solar Cell with Electron-Selective TiO_2 Contact. *ACS Photonics* **1**, 1245–1250 (2014).
20. Kashiwaya, S. *et al.* The Work Function of TiO2. *Surfaces* **1**, 73–89 (2018).
21. Jellison, Jr, G. E. Spectroscopic ellipsometry data analysis: measured versus calculated quantities. *Thin Solid Films* **313–314**, 33–39 (1998).
22. Shi, Y.-J. *et al.* Optical Constants and Band Gap Evolution with Phase Transition in Sub-20-nm-Thick TiO2 Films Prepared by ALD. *Nanoscale Res. Lett.* **12**, 243 (2017).
23. Yang, X. *et al.* High-Performance TiO2-Based Electron-Selective Contacts for Crystalline Silicon Solar Cells. *Adv. Mater.* **28**, 5891–5897

24. Zhao, J., Wang, A., Altermatt, P. & Green, M. A. Twenty-four percent efficient silicon solar cells with double layer antireflection coatings and reduced resistance loss. *Appl. Phys. Lett.* **66**, 3636–3638 (1995).
25. D.E. Kane & Swanson, R. M. Measurement of the Emitter Saturation Current by a Contactless Photoconductivity Decay Method. in *Proc of the 18th IEEE Photovoltaic Specialists Conference* 578–583 (1985).
26. Fell, A., Fong, K. C., McIntosh, K. R., Franklin, E. & Blakers, A. W. 3-D Simulation of Interdigitated-Back-Contact Silicon Solar Cells With Quokka Including Perimeter Losses. *IEEE J. Photovolt.* **4**, 1040–1045 (2014).
27. NIST X-ray Photoelectron Spectroscopy Database, NIST Standard Reference Database Number 20, National Institute of Standards and Technology, Gaithersburg MD, 20899, 2000. Available at: https://srdata.nist.gov/xps/main_search_menu.aspx. (Accessed: 18th October 2018)

nd Al contacts and the inset shows a schematic of the TLM structure used in the ρc extraction.

riation shown in Fig. 1c or the estimated error in the TLM measurement (whichever is largest).

presents the modelled contribution from different oxidation states to the measured spectrum.

sign and the integrated short circuit current is also listed. The white scale bar represents 1cm.

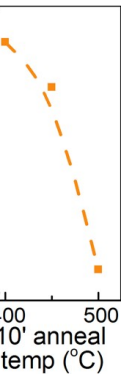

ell. **b,** change in efficiency of the n-type PRC cell as a function of anneal time and temperature.

An electron-selective TiO_x based heterocontact is developed and trialed as a dopant-free partial rear contact in high efficiency silicon solar cells. This cell not only reaches an efficiency of above 23% but also maintains its performance after a short anneal at 400°C – setting new benchmarks of performance and thermal stability for this cell architecture.

Keywords: Titanium oxide, selective contacts, silicon photovoltaics

J. Bullock, Y. Wan, M. Hettick, X. Zhaoran, S. P. Phang, D. Yan, H. Wang, W. Ji, C. Samundsett, Z. Hameri, D. Macdonald, A. Cuevas and A. Javey*

Title Dopant-Free Partial Rear Contacts Enabling 23% Silicon Solar Cells

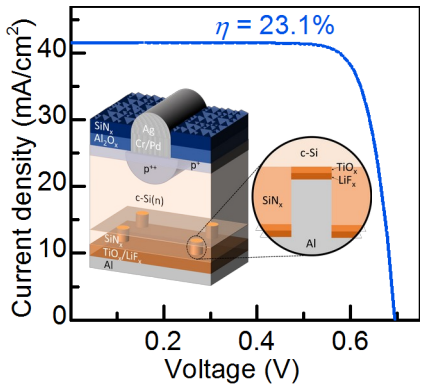

Supporting Information

Title Dopant-Free Partial Rear Contacts Enabling 23% Silicon Solar Cells

James Bullock, Yimao Wan, Mark Hettick, Xu Zhaoran, Sieu Pheng Phang, Di Yan, Hanchen Wang, Wenbo Ji, Chris Samundsett, Ziv Hameri, Daniel Macdonald, Andres Cuevas and Ali Javey*

S1: Cell optical analysis

To compare the rear reflection performance of the TiO_x / LiF_x / Al contact against Mg and Ca based contacts a series of simulations were performed using the program *Wafer ray tracer* hosted by *PVLighthouse.com*. The layers used in the simulations are shown at the bottom of Figure S1a and are chosen to mimic the structure of the 23.1% cell in the main text. The three simulations show the maximum short circuit current density (orange) as well as remainder loss mechanisms due to absorption in the rear films (black) and loss out of the front surface (blue). The TiO_x / LiF_x / Al contact produces the lowest rear-side losses (by more than 1 mA/cm^2 in comparison to the Ca based contact). This benefit is not fully translated to the short circuit current density as the improved rear reflection also results in an increase in the amount of longer wavelength light lost instead through the front surface. In other simulations (not shown), the very thin TiO_x and LiF_x layers are found to have a negligible effect on the optics of the cell.

The rear side reflection could potentially be further improved using a TiO_x / LiF_x / Al / Ag contact where the Al layer is thin enough to have a reduced optical impact while being thick enough to produce a low resistivity contact. Figure S1b shows the simulated short circuit current density as a function of thickness of the Al layer. A clear trend of improving current density is simulated with decreasing Al thickness. However, even with 0 nm of Al, corresponding to the near ideal reflection of silver in this wavelength region, a maximum improvement of only 0.16 mA/cm^2 is seen. This small gain is unlikely to offset the added complexity associated with its integration.

S2: Additional contact resistance analysis

To investigate the influence of the LiF_x layer in the TiO_x / LiF_x / Al heterocontact, a series of simple contact test structures are fabricated on 1 Ωcm n-type wafers with and without LiF_x interlayers (a schematic of these structures is provided in the inset of Figure S2a). Total resistance R_{total} measurements were taken between sets of pads, separated by a common distance d. Figure S1a shows a comparison R_{total} for samples which differ by the thicknesses of a TiO_x layer (1.5, 3 and 6 nm) and the presence of a LiF_x layer (~1 nm), both deposited underneath the Al pads. It can be seen that the R_{total} increases with the thickness of the TiO_x layer in both samples with and without LiF_x, likely a result of a large bulk resistivity of TiO_x. In addition, the use of LiF_x results in a dramatic reduction of the R_t, especially in the case of thicker TiO_x layers, this suggests that the known low work function of the LiF_x / Al electrode can reduce the total resistivity of the contact. We note that

simple two-pad contact test structures were used in this comparison as the prohibitively high resistivity of the TiO_x / Al contacts prevented usage of full transfer-length method measurements.

A second plot which highlights the thermal stability enhancement resultant from the addition of the TiO_x layer is provided in Figure S2b. The plot shows the evolution of contact resistivity with increased annealing temperatures between samples with and without the TiO_x layer. The TiO_x / LiF_x / Al sample (blue) shows a slight decrease in contact resistivity at higher temperatures whereas the LiF_x / Al sample (purple) shows a dramatic increase in contact resistivity at ~200^{o}C.

Figure S1: a, current density analysis of three rear contact schemes showing the superior opt

ct and a TiOx / LiFx / Al heterocontact (blue) showing significantly higher stability for the latter.